iScience

Article

Phenotypic consequences of logarithmic signaling in MAPK stress response

Graphical abstract

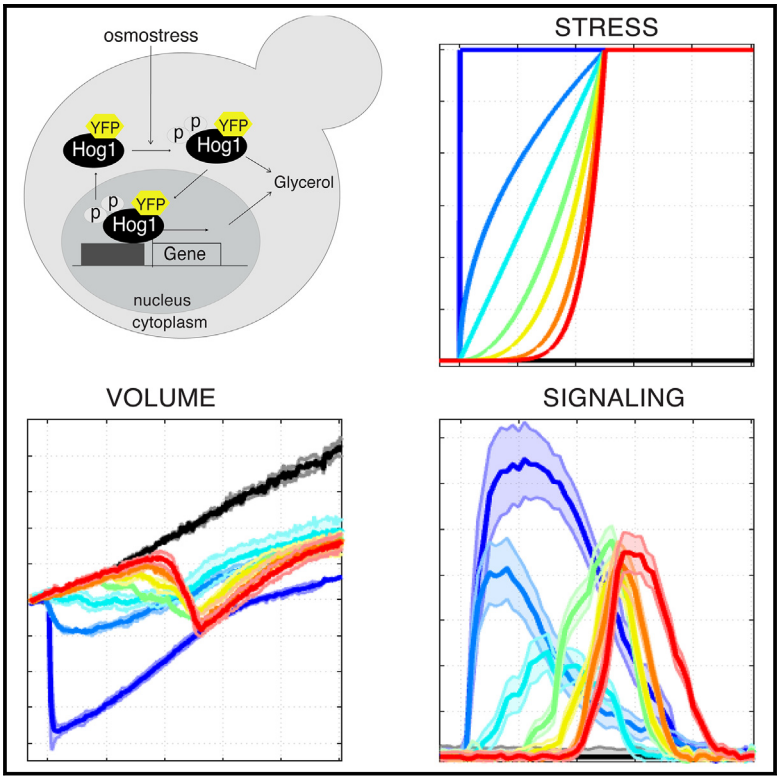

Highlights

- Gradual stress enhances cell growth compared to acute stress conditions
- Growth advantage links to minimal cell volume reduction during gradual stress
- Logarithmic signaling underpins the yeast MAPK osmotic stress response
- Study advances understanding of cell signaling and growth in dynamic environments

Authors

Hossein Jashnsaz, Gregor Neuert

Correspondence

hjashnsaz@gmail.com (H.J.),
gregor.neuert@vanderbilt.edu (G.N.)

In brief

Biocomputational method; Cell biology

Jashnsaz & Neuert, 2025, iScience *28*, 111625
January 17, 2025
https://doi.org/10.1016/j.isci.2024.111625

CellPress

iScience

CellPress
OPEN ACCESS

Article

Phenotypic consequences of logarithmic signaling in MAPK stress response

Hossein Jashnsaz[1,*] and Gregor Neuert[1,2,3,4,*]
[1]Department of Molecular Physiology and Biophysics, School of Medicine, Vanderbilt University, Nashville, TN 37232, USA
[2]Department of Pharmacology, School of Medicine, Vanderbilt University, Nashville, TN 37232, USA
[3]Department of Biomedical Engineering, School of Engineering, Vanderbilt University, Nashville, TN 37232, USA
[4]Lead contact
*Correspondence: hjashnsaz@gmail.com (H.J.), gregor.neuert@vanderbilt.edu (G.N.)
https://doi.org/10.1016/j.isci.2024.111625

SUMMARY

How cells respond to dynamic environmental changes is crucial for understanding fundamental biological processes and cell physiology. In this study, we developed an experimental and quantitative analytical framework to explore how dynamic stress gradients that change over time regulate cellular volume, signaling activation, and growth phenotypes. Our findings reveal that gradual stress conditions substantially enhance cell growth compared to conventional acute stress. This growth advantage correlates with a minimal reduction in cell volume dependent on the dynamic of stress. We explain the growth phenotype with our finding of a logarithmic signal transduction mechanism in the yeast mitogen-activated protein kinase (MAPK) osmotic stress response pathway. These insights into the interplay between gradual environments, cell volume change, dynamic cell signaling, and growth, advance our understanding of fundamental cellular processes in gradual stress environments.

INTRODUCTION

Signal transduction is fundamental for a variety of cellular processes, including growth, differentiation, migration, and programmed cell death.[1] These complex pathways play a pivotal role in maintaining normal cellular functions, and disruptions in their regulation can result in developmental defects and various human diseases.[2–6] Despite the wealth of knowledge on individual proteins and signaling pathways, accurately predicting how cells respond to a range of perturbations, such as environmental changes and drug treatments, remains a formidable challenge.[7–9]

The complexity of cell signaling is heightened by its spatiotemporal dynamics, yet current cell biology often simplifies this by studying a limited number of pathway components under steady-state conditions or during abrupt shifts between constant concentrations..[10–12] In their physiological context, cells experience stress concentrations that change in diverse ways—sudden, linear, nonlinear, or repetitive—over time, space, or both.[13,14] These variations occur on timescales and spatial scales distinct from abrupt transitions between constant levels.[15] For instance, circadian oscillations happen once per day, synaptic firing occurs multiple times per second, and hormones like insulin display unique temporal patterns that regulate intracellular processes based on their dynamics.[16] Unlike acute changes, these physiological variations can occur gradually over time or space, creating a mismatch between traditional experimental approaches and the dynamic nature of real physiological environments, thereby limiting our understanding of signaling behavior in complex natural settings.[15]

Emerging studies show that variations in cell stimulations over time or space can significantly alter intracellular signaling dynamics.[15,17] Differences in signal amplitude, duration, rate, or oscillation can lead to changes in gene expression or distinct cell phenotypes.[5,13–29] These stimulations range from extracellular cues like growth factors[30] and stressors[19,31,32] to intercellular molecules such as morphogens,[5,23,33] cytokines,[34–38] hormones,[16] and neurotransmitters,[39] and even intracellular signals like DNA damage[40] or cell cycle factors.[21] The diverse responses to different temporal or spatial patterns of the same signal reveal a critical gap in understanding signaling mechanisms in gradual, physiological environments.

We developed a method to mimic physiological environments by gradually changing stress concentrations around individual cells.[13,14,24,26] This approach has proven more effective than conventional methods for building predictive models of cell signaling.[13,14] Studies, including ours, have examined how varying the rate of osmotic stress affects signaling and cell survival.[15,17,20,23–26,40–43] However, how cells continuously integrate dynamic stress features over time, including rate and concentration, and how gradual stress influences cell morphology and growth, remains poorly understood.

This study examines how acute stress and gradual physiological stress differently affect signaling and cell growth, focusing on how cells integrate gradual environmental changes over time. Using the conserved Mitogen-Activated Protein Kinase (MAPK) High Osmolarity Glycerol (HOG) stress signaling pathway in yeast *Saccharomyces cerevisiae*,[44,45] we developed an experimental and analytical framework to study dynamic volume changes and

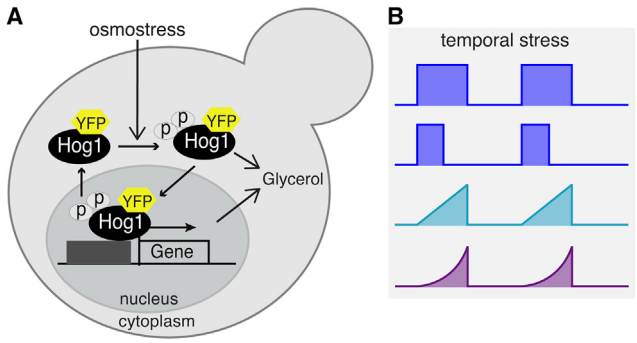

Figure 1. Dissecting Osmostress regulation of volume change, cell growth and Hog1 signaling

This figure presents an illustration of the conventional Hog1 signaling in yeast stress response pathway and our proposed gradual stress paradigms.

(A) In accordance with the established model of osmotic stress regulation in yeast, that is based on acute stress, osmotic stress activates Hog1 signaling and inhibits cell growth in an osmotic concentration stress dependent manner. Osmotic stress triggers the activation of and double phosphorylation of Hog1 MAPK, via the HOG signal transduction pathway. Dual Hog1 phosphorylation leads to its translocation to the nucleus, where it regulates stress-responsive genes. The concerted action of Hog1 phosphorylation and the gene responses contributes to the regulation of glycerol production and maintenance, facilitating osmoadaptation.

(B) We applied different stress paradigms including acute (blue) and gradual (cyan and purple) changes to investigate the relationship between osmotic stress, cell volume change, Hog1 signaling, and cell growth.

signaling processes. Our findings reveal that rate sensing and logarithmic signaling play key roles in eukaryotic MAPK transduction, enabling cells to process dynamic stress over time.

The Hog1 pathway, highly conserved across species, is crucial for osmotic stress responses, making it ideal for exploring cellular adaptation to gradual environmental changes.[14,26,32,44–49] Research shows that severe osmotic stress reduces cell volume, slowing Hog1 transduction due to molecular crowding, which impacts processes like growth.[45–47] Using controlled gradual stress, we measured cell volume, Hog1 nuclear localization, and growth, finding optimal growth under gradual severe stress and uncovering logarithmic signaling as a mechanism for detecting relative extracellular stress changes (Figure 1A).[50–53]

Unlike transient Hog1 activation under acute stress, gradual stress resulted in either Hog1 signaling decay (linear stress) or sustained activation (exponential stress). These distinct dynamics, differing from models based solely on concentration or rate changes, deepen our understanding of how cells adapt to gradual environmental changes.

RESULTS

Gradually rising stress conditions compared to acute and pulsatile stress conditions result in growth advantage

Here, we study how gradual stress impacts the cellular growth phenotype. Our findings revealed a strong correlation between the stress gradient type and cell growth. Standard yeast stress response models suggest that the severity (concentration or duration) of stress directly influences the cell growth phenotype.[19,50,51,53] We exposed cells to an acute stress in the form of a 3M pulsatile NaCl for 120 min and subsequently quantified the cell doubling time after exposure as 453 ± 46 min (Figures 2A and 2B, STAR Methods). In comparison, exposure of cells to acute 3M NaCl stress for 30 min resulted in a cell doubling time of 218 ± 18 min (Figures 2C and 2D, STAR Methods). Next, we exposed cells to a linear increasing stress (3M NaCl in 120 min), and measured a reduced cell doubling time of 147 ± 16 min (Figure 2E). Exposing cells to an exponential increasing stress scenario of the same intensity and duration reduced the cell doubling time to 117 ± 1 min (Figure 2F). Our investigation unveiled a remarkable deviation from the acute step and pulse stress profiles and phenotypes. The type of gradual stress proved to be a pivotal factor in determining the cell growth phenotype even more than stress intensity, duration, or total stress (integrated stress exposure quantified as the total area under the stress profile) (Figures 2G–2I). Our results indicate that cells grow substantially better under gradually rising stress conditions compared to acute pulsatile stress conditions(Figure 2, purple a cyan compared to blue) even for stressor with a similar total stress exposure (Figure S1C vs. J). These observations are even more prevalent in repetitive stress conditions after exposure to a second stress treatment (Figures 2 and S1). This intriguing outcome sheds light on the intricate interplay between the gradual aspects of stress and cellular responses, highlighting the significance of gradual stress exposure in enhancing cell growth.

Gradual stress of single cells results in distinct cell volume phenotypes and Hog1 signaling dynamic responses

To understand the observed cell growth phenotypes, we implemented gradual stress paradigms and quantified cell volume changes and Hog1 signaling activation via time lapse microscopy. We aimed to elucidate these dynamics by employing precisely controlled gradual concentration profiles, contrasting them with acute stress implemented as instant step-like concentration changes. The gradual concentration profiles, implemented as polynomial functions of time (Figure 3A), were characterized by three key parameters: C_{max} (maximum concentration change), T (stress duration), and k (polynomial order), which governed how the profile reached C_{max} over T (Figure 3B). In these profiles, k = 1 represented linear stress, while k values between zero and one signified stress starting with the highest rate and gradually decreasing (Figure 3A). For k > 1, stress started with slower rates and increased over time. Additionally, we generated exponentially increasing profiles akin to the polynomial ones, beginning at 0 and reaching C_{max} over T (Figure 3B).

In our experimental setup, we compared the responses to a 0M NaCl control and an acute 0.6M NaCl stress at t = 0 min with the responses to polynomial NaCl increases from zero to 0.6M over 25 min for k values of 0.5, 1, 2, 3, 5, and 7 (Figure 3C). These concentrations were then maintained at 0.6M for an additional 25 min (Figure 3C). Subsequently, we applied these stress profiles to single cells (Figure 3D) and conducted real-time measurements to quantify cellular volume changes over time (Figure 3E) and Hog1 nuclear localization (Figure 3F) during the stress periods using time-lapse microscopy (Figure S2).

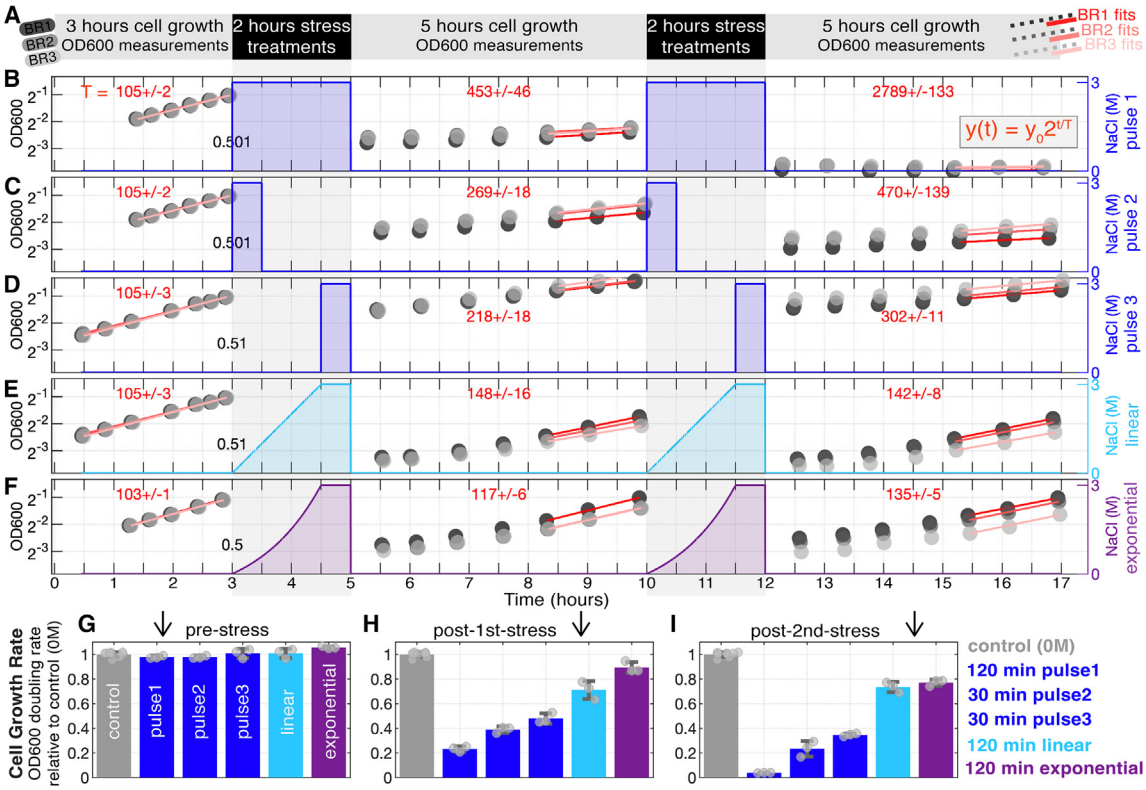

Figure 2. Enhanced cell growth under gradual osmotic stress compared to acute pulsatile stress

(A–F) We evaluated cell growth under various NaCl stress conditions through OD600 measurements of yeast cell cultures. (A) Cells were initially grown to an exponential phase (OD600 = 0.5) before being subjected to repetitive 3M NaCl osmotic stresses, including (B) a 120-min long pulse, (C) a 30-min pulse, (D) a 30-min pulse starting at t = 90 min from the start of treatment period (a control for cell density, see STAR Methods), (E) a 120-min linear profile (cyan), and (F) a 120-min exponential profile (purple). The linear and exponential stress profiles gradually increased to 3M over 90 min, remaining at this concentration for an additional 30 min. Following each 2-h stress treatment, cells were filtered to remove NaCl, resuspended in fresh growth media, and their OD600 was monitored for 5 h in 3 biological replicates (black, gray, light-filled circles in (B.–F.). After 5 h, the stress treatments and OD600 measurements were repeated. The OD600 measurements were fitted to exponential growth curves (B–F), depicted on a log2 y axis in red over time, and fits utilized the last three timepoints. Cell growth doubling times were calculated from each fit (indicated by red numbers rounded to the nearest minute). The values provided at t = 3 h at the onset of the initial 2-h stress treatment in (B–F) represent OD600 estimates derived from fits applied to pre-stress OD600 measurements. An approximate value of 0.5 indicates that all conditions maintained a similar initial cell density at the beginning of the 2-h stress treatment period.

(G–I) Cell growth rates, relative to the control (0M, no stress), were determined for (G) pre-stress, (H) post 1st stress treatments, and (I) post 2nd stress treatments based on OD600 doubling rates. Errorbars are mean and standard deviation from three biological replica experiments. Further details can be found in Figure S1.

Our results unveiled significant distinctions in cellular responses to these dynamic stress profiles even though all concentrations reached the same final values and some have even similar total integrated stress exposure (Figure S1C, S1J, and S6). Under growth media with 0M NaCl, cellular volume showed gradual expansion and an overall increase over time (Figure 3E). In contrast, an acute NaCl stress led to a rapid and substantial reduction in cellular volume. Gradual increases in stress resulted in different and sustained cell volume reductions over time for the duration of the stress (Figure 3E).

At the signaling level, we observed distinct patterns of Hog1 nuclear localization (defined as $Hog1^{nuc}$) in response to these stress profiles (Figure 3F). In growth media with 0M NaCl, there was no discernible change in Hog1 nuclear localization. Conversely, an acute NaCl stress induced a rapid and robust transient increase in Hog1 nuclear localization. Gradual NaCl stress, however, elicited delayed Hog1 activity that did not reach the maximum activation observed under an acute stress. Furthermore, the timing of maximum activation was shifted, and all activities ultimately adapted to pre-stress levels over a 50-min period.

Both in terms of cellular morphology and signaling dynamics, responses to gradual stress exhibited marked differences between conditions over time. These findings underscore the nuanced and distinct cellular responses arising from variations in gradual stress profiles.

Cell volume reduction and Hog1 nuclear localization follow the change in stress dynamics with high fidelity

Here, we focused on quantifying the precision and fidelity of cellular responses following the gradual stress profiles, particularly their impact on cell volume reduction and Hog1 nuclear localization. Under gradual NaCl stress, with final concentrations set at C_{max} = 0.6M (Figure 4A), we observed distinct patterns in

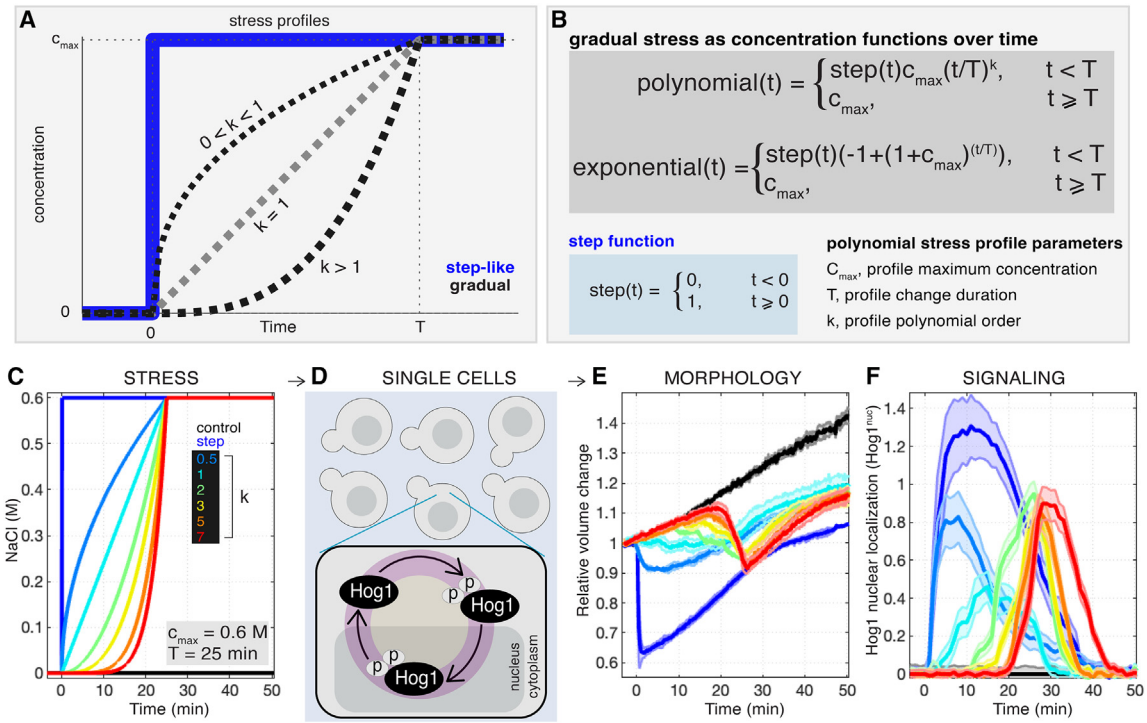

Figure 3. Distinct responses to gradual stress in single cells

(A) We employed gradual stress concentration increases over time, contrasting them with acute, step-like stress at time zero.

(B) Gradual stress followed polynomial increases over time, with profiles reaching the final concentration (C_{max}) over a specified duration (T), determined by the polynomial order (k). Exponential increases were also considered.

(C) Gradual NaCl stress profiles according to polynomial increases are applied to (D) yeast cells resulted in distinct (E) cell volume relative changes and (F) Hog1 kinase nuclear localization dynamics ($Hog1^{nuc}$) phenotypes. Gradual NaCl concentration profiles in (C) followed various functions, including step (t^0), root ($\sqrt{t}$), linear (t^1), quadratic (t^2), cubic (t^5), quintic (t^5), and haptic (t^7), each reaching a final concentration of 0.60 NaCl over 25 min, all compared to a no-salt control (0M). The thick lines and shaded areas in (E), (F) represent the mean and standard deviation (std) from 2 or 3 biological replicates, each consisting of approximately 100 single cells observed through live cell time-lapse microscopy. Further details can be found in Figure S2.

relative cell volume change (Figure 4B) and cell volume reduction (Figure 4C) phenotypes. We define cell volume reduction as the volume change under each NaCl stress condition relative to the volume change in growth media of 0M NaCl condition.

The maximum cell volume reduction (Figure 4D) and the total cell volume reduction over the 25-min stress time (Figure 4E) exhibited marked variations among the stress conditions. The former represents the highest reduction in cell volume, while the latter denotes the integrated cell volume reduction throughout the 25 min of cell stress. Notably, step-like stress resulted in the highest cell volume reductions among all the gradual stress profiles. In contrast, both linear and exponential stress led to the lowest (total or maximum) cell volume reduction when compared to other gradual stress. Furthermore, our analysis revealed a negative correlation between cell growth rate and cell volume reductions under osmotic stress conditions (Figure 4F).

Next, we quantified the dynamics of both cell volume reduction and Hog1nuc compared to NaCl stress change by fitting each volume and Hog1 response to a polynomial function (Figures 4G, S3, S4, and Table 1, STAR Methods). We found that cells process the stress change at volume level different than that of Hog1 activation. For example, in response to a quadratic stress change over time (k = 2), cell volume reduction follows a polynomial change of smaller order (k = 1.86) while Hog1nuc follow a polynomial change of greater order (k = 3.15) (Figure 4G). This observation suggests a specific mathematical relationship between the applied gradual stress and the resulting cell volume changes and Hog1nuc dynamics.

To answer whether Hog1nuc activity impacts cell volume reduction, we directly compared the dynamics of $Hog1^{nuc}$ to that of cellular volume reduction under gradual NaCl stress (Figure 4G). Like acute stress conditions,[20] we observed that $Hog1^{nuc}$ dynamics is delayed relative to cell volume reduction dynamics under all gradual stress conditions (Figure 4G). This observed delay in $Hog1^{nuc}$ dynamics suggest that $Hog1^{nuc}$ dynamics does not impact cell volume reduction. Rather, the observed cell volume reduction is a direct consequence of extracellular stress change, irrespective of $Hog1^{nuc}$ activity.

These results collectively emphasize the fidelity of cellular responses to gradual stress changes, offering valuable insights into the relationship and the temporal order among extracellular stress change, cell volume dynamics, signaling activation, and cell growth phenotypes. This raises the question why do the linear and exponential profiles cause minimal volume change and enhanced growth after stress.

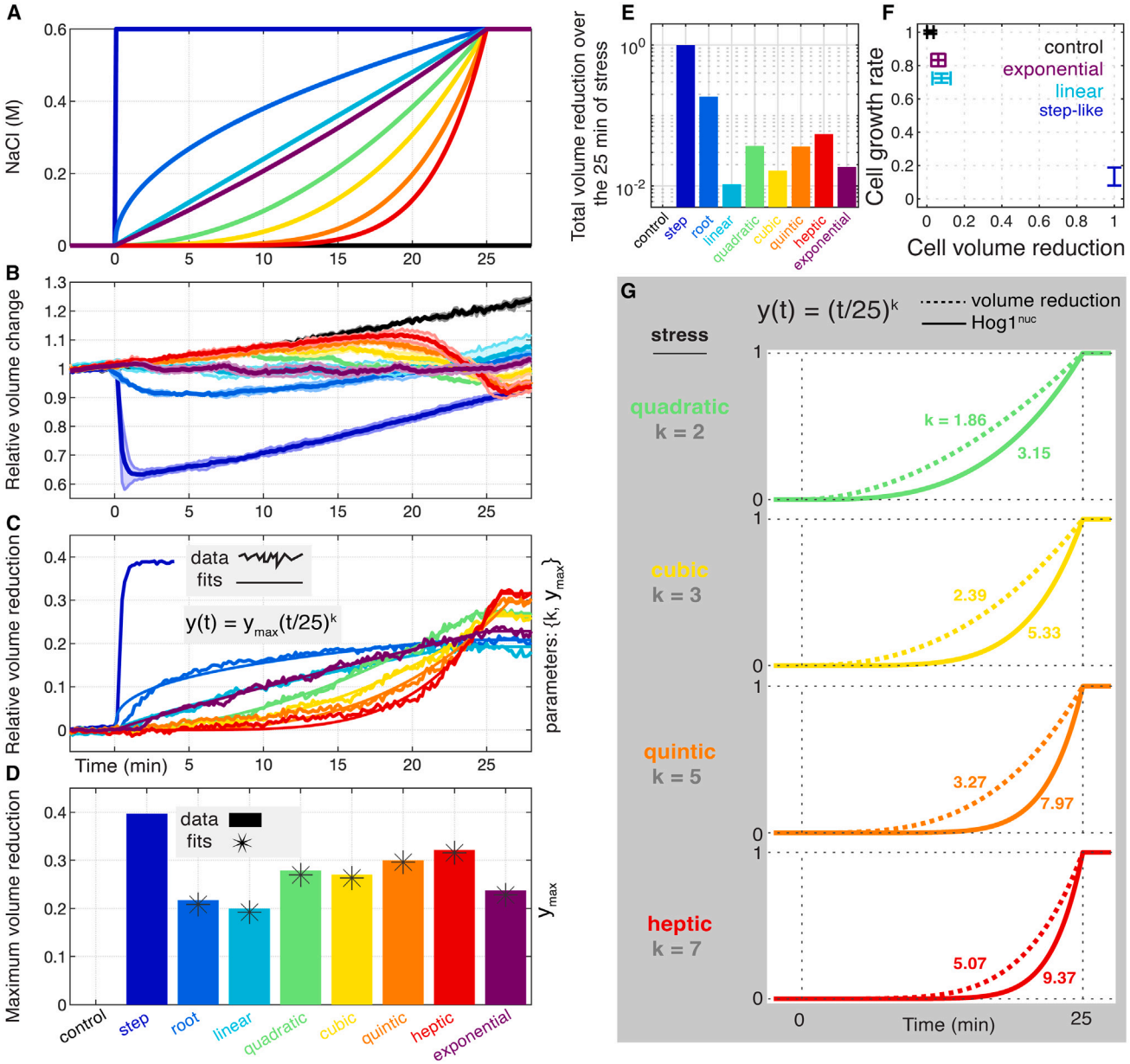

Figure 4. Dynamic cellular responses to gradual NaCl stress

(A) Gradual NaCl stress were applied to yeast cells, with final concentration of C_{max} = 0.6M, resulting in differential (B) relative cell volume changes and (C) cell volume reduction, defined as the volume change under each stress condition relative to that under the no-salt condition. The thick lines and shaded areas in (B) represent the mean and standard deviation (std) from 2 or 3 biological replicates, each consisting of approximately 100 single cells observed through live cell time-lapse microscopy.

(D) The maximum cell volume reduction and (E) the total cell volume reduction over the 25-min stress period exhibited variability across different gradual stresses.

(F) Cell growth showed a negative correlation with cell volume reduction amount, including both maximum and total reduction. The x axis displays the mean and standard deviation (std) of volume reduction values (both maximum and total reductions) under control, step, linear, and exponential stress for five different final concentrations (C_{max} = 0.1M, 0.2M, 0.4M, 0.6M, and 0.8M), each normalized to the step condition with the greatest cell volume reduction (see Figure S3E). The y axis illustrates the mean and std of cell growth rates under control, step, linear, and exponential stress conditions, normalized to the control condition with the highest cell growth rate values. Values from three biological replicates at post-1st-stress and post-2nd-stress are aggregated for this quantification (see Figures 2G–2I).

(G) The dynamics of Hog1 nuclear localization (Hog1^{nuc}) were delayed concerning cell volume reduction dynamics under all stress changes. Further details can be found in Figures S3 and S4.

Table 1. Statistics of the biological replicates and single cells

		Final concentrations				
		0.10M	0.20M	0.40M	0.60M	0.80M
Gradual stress type	steps (t^0)	(1, 78)	(3, 324)	(3, 487)	(3, 407)	(3, 476)
	root2 ($\sqrt{t}$)	(1, 64)	(2,183)	(2, 221)	(2, 285)	(2,326)
	linears (t^1)	(1, 98)	(2, 195)	(2, 211)	(2, 195)	(2, 307)
	quadratics (t^2)	(1, 102)	(2, 175)	(2, 170)	(2, 243)	(2, 247)
	quints (t^5)	(1, 62)	(3, 252)	(3, 347)	(3, 388)	(2, 282)
	haptics (t^7)	(1, 69)	(3, 285)	(3, 247)	(3, 264)	(2, 276)
	Exponential (a^t)	(1, 71)	(2, 238)	(2, 216)	(2, 237)	(2, 210)

For each condition, the first number represent the number of biological replicates, and the second number indicate an approximate number of total single cells from all biological replicates for that condition.

Logarithmic signaling mediates a response proportional to the relative changes of extracellular environment

To address this question, we aim to better understand how gradual stress profiles control Hog1 signaling dynamics by means of phenomenological predictive modeling with the aim to identify a signaling mechanism. We conducted a comprehensive analysis that compared the behaviors of linear signaling (or rate sensing) models, where the cellular response is directly proportional to the rate of change in the stress, with logarithmic signaling models, in which the response is proportionate to the relative change in stress with respect to the perceiving background concentration over time. Additionally, we explored a hybrid model that incorporated equal contributions from both linear and logarithmic signaling responses additively (see STAR Methods). To dissect the unique characteristics of these signaling mechanisms, we subjected each of the linear, logarithmic, and hybrid models to four distinct cell stress paradigms (Figure 5).

In the linear stress paradigm, cells encountered a stress that exhibited linearly increasing concentration at a consistent rate over time (Figure 5A). Our analysis predicted distinct responses under each of the three signaling mechanisms studied. Following reaching the maximum level, we predicted that the response would exhibit constant (Figure 5B), gradual decay (Figure 5C), and slower decay (Figure 5D) characteristics over time within the linear, logarithmic, and hybrid models, respectively. It's worth noting that the hybrid model was expected to display a slower rate of decay in response compared to the logarithmic mechanism, while the linear signaling mechanism to maintain a constant response level.

In the exponential stress paradigm, cells were exposed to stress that exponentially increased in concentration over time (Figure 5E), resulting in response dynamics as follows: after the initial rise, the response was expected to show increasing, constant, and slower increasing patterns over time within the linear (Figure 5F), logarithmic (Figure 5G), and hybrid (Figure 5H) models, respectively. In each of the three signaling mechanisms, the response to an exponentially increasing stress was projected to persist at a higher level compared to the response to a linearly increasing stress.

In the pulsatile stress paradigm, cells received repeating acute stress (Figure 5I), leading to identical responses throughout the stress periods (constant responses at each pulse of stress application) across all signaling mechanisms (Figures 5J–5L). Notably, pulsatile stress did not yield distinctive responses among the signaling mechanisms, indicating their inability to discern between them.

In the staircase stress paradigm, the cells experienced a stress that followed a staircase pattern, with a constant step change at each period without switching back to pre-stress level (Figure 5M). Staircase stress differentiated between the three signaling mechanisms. The linear signaling is predicted to lead to cellular responses that remained constant throughout the stress periods (Figure 5N). On the other hand, the logarithmic and the hybrid signaling mechanisms both are predicted to lead to cellular responses that decayed throughout the stress periods (Figures 5O and 5P).

In addition to these four major cell stress paradigms and to further test different signaling paradigms, we also considered polynomial cell stress similar to those in Figure 3C. The Taylor series summation of polynomials stress profiles of order k = 1,2,3,5,7 (the Maclaurin series expansion for an exponential function with coefficients as 1/k!, where k! represents the factorial of k) recapitulates an exponentially increasing stress profile (Figure 5Q compared to Figure 5E). We quantified the responses to each polynomial stress through each of the models. Similar summations of signaling responses to polynomial stress recapitulated responses consistent with those observed with exponential stress (Figures 5R–5T compared to Figures 5F–5H). Next, we experimentally validate these predictions to differentiate between linear, logarithmic, and hybrid signaling mechanisms.

Implementing gradual cell stress confirmed that logarithmic signaling contributes to the HOG pathway signaling response

In our experimental investigations, we employed various gradual cell stress conditions to illuminate the signaling behavior of the HOG pathway. Specifically, we examined the response of yeast cells to different forms of gradual NaCl stress at varying final concentrations. A summary of key findings are as follows:

Linear stress, characterized by a gradual increase in NaCl concentration with a constant rate over time to two different final concentrations of C_{max} = 0.6M and 0.8M (Figure 6A), induced a pattern of increasing cell volume reduction over time (Figure 6B). Quantification of these results indicates that cell volume change follows a polynomial function of order less than k = 1 for the linear

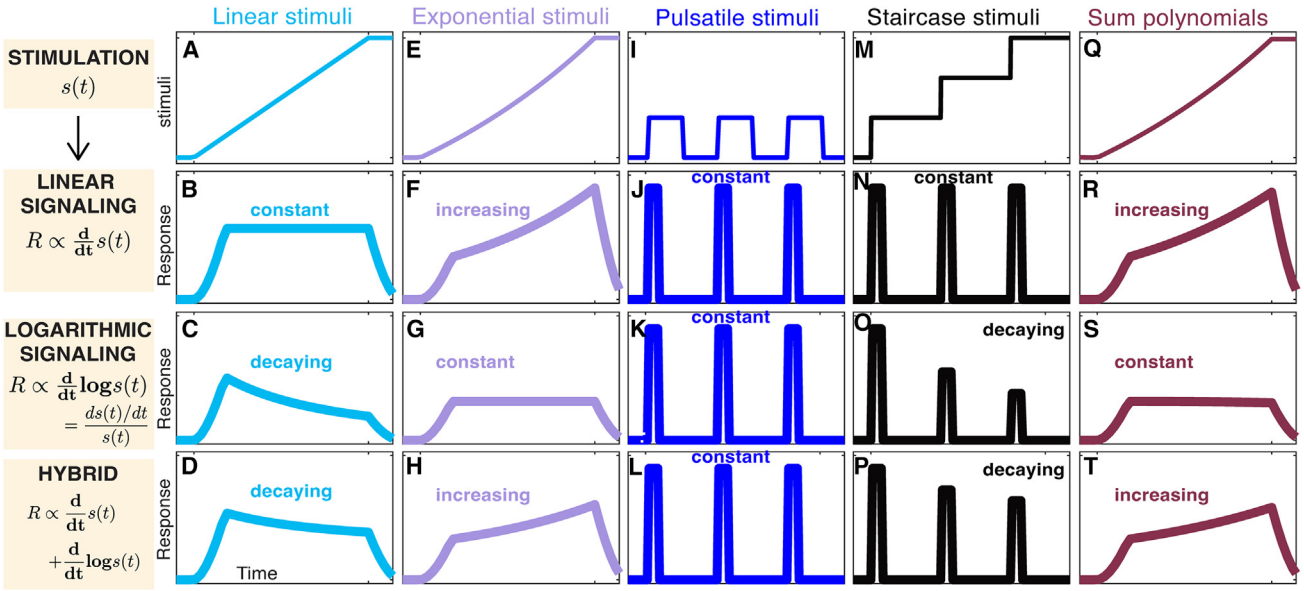

Figure 5. Different signaling models convert gradual environmental changes into different signaling responses

(A) Under a linear stress, the three models produce (B) constant, (C) decaying, and (D) slower decaying responses over time within the linear, logarithmic, and hybrid models, respectively.

(E) An exponential stress results in (F) increasing, (G) constant, and (H) slower increasing responses over time within the three models, respectively.

(I) Pulsatile stress induces (J.–L.) responses that remain constant throughout the stress periods across all three signaling models. (M) A staircase stress mediates (N) constant, (O) decaying, and (P) slower decaying responses throughout the stress periods within the three models. The Taylor series summation of polynomials stress of order k = 1,2,3,5,7 (the Maclaurin series expansion for exponential stress, see STAR Methods) is illustrated in (Q). Similar summations of signaling to polynomial stress generate (R.–T.) responses consistent with those observed with exponential stress. The responses are smoothed over 3 timepoints for each model. Further details can be found in the STAR Methods section.

stress (Figures S3D–S3F, cyan). In parallel, this linear stress paradigm resulted in decaying Hog1^{nuc} dynamics after reaching the maximum level (Figure 6C, decaying trend are indicated via black lines). Exponential stress, where the NaCl concentration increased exponentially reaching two different final concentrations of C_{max} = 0.6M and 0.8M each over 25 min (Figure 6D), led to a linear increase in cell volume reductions (Figures 6E and S3D–S3F, purple), and an increase in Hog1^{nuc} activity over the course of stress (Figure 6F). These stress paradigms together show that the Hog1 pathway behaves as a hybrid model that combines both rate sensing and logarithmic sensing mechanisms (Figures 5D and 5H).

To further explore the response patterns, we quantified the sum of the transient Hog1^{nuc} responses induced by polynomial stress of various orders (k = 1,2,3,5,7) (Figure 6G). We performed these sums using weight coefficients according to the Maclaurin series expansion (see STAR Methods). Surprisingly, these responses closely resembled those observed under exponential stress, characterized by linearly increasing cell volume reduction and increasing Hog1^{nuc} dynamics over time (Figures 6H and 6I).

Finally, we examined the effects of two distinct stress types: pulsatile and staircase. Pulsatile stress consisted of three identical acute stresses between 0 and 0.2M NaCl (Figure 6J, blue line), while staircase stress followed a sequential, constant change of 0.2M, without changing back to 0 (Figure 6J, black line). These stresses resulted in differential dynamics for both cell volume reduction and Hog1^{nuc} responses over time (Figures 6K, 6L, and S5).

Comparing the observations on Hog1 responses under the five distinct NaCl stress paradigms, namely Linear, Exponential, Sum of Polynomials, Pulsatile, and Staircase Stress, to the quantitative results obtained from different models, confirmed that the Hog1 pathway performs signaling according to a hybrid model (a sum of linear signaling and logarithmic signaling) in response to gradual NaCl stress (Figures 6C, 6F, 6I, and 6L compared to Figures 5D, 5H, 5L, 5P, and 5T). These findings collectively confirm that the HOG pathway operates at a signaling mode that incorporates both a linear signaling and a logarithmic signaling mechanism in response to gradual environmental changes. The distinct response patterns observed under different stress conditions highlight the pathway's ability to perceive and transduce gradual changes in its environment, providing valuable insights into its role in cellular signal transduction.

DISCUSSION

In this study, we implemented gradual stress profiles and quantified dynamic cellular responses under a wide range of conditions. This general approach is a significant development toward a quantitative investigation of dynamic signaling processes, including mechanistic understanding of cell signaling in physiologic cellular environments. We found that cells grow substantially better under gradually rising stress compared to acute and

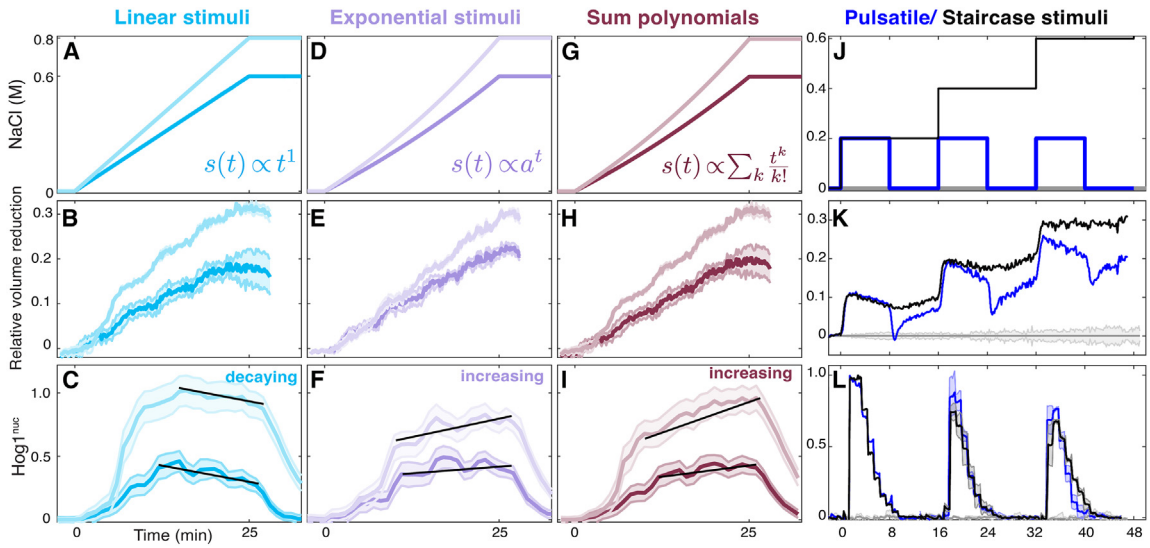

Figure 6. Verification of Logarithmic Signaling in the HOG Pathway through Gradual Cell Stress

(A) Linear NaCl stress (with final concentrations of C_{max} = 0.6M and 0.8M) lead to (B) increasing cell volume reduction and (C) decaying dynamics of Hog1 nuclear localization over time.

(D) Exponential stress result in (E) increasing cell volume reduction and (F) increasing Hog1nuc dynamics over time. Fitting cell volume reduction to a polynomial function indicates that volume reduction changes with a smaller polynomial order under linear stress compared to exponential stress (see Figures S3D and S3F for C_{max} = 0.6M and 0.8M).

(G–I) Summation of cell volume reduction dynamics and the transient responses of Hog1nuc to NaCl stress with polynomial orders (k = 1,2,3,5,7) generated (H) increasing cell volume reduction and (I) increasing Hog1nuc dynamics over time, similar to the responses observed with exponential stress at each final concentration. (J) A comparison between pulsatile and staircase NaCl stress, consisting of three equal-height step elevations, shows differential dynamics in both (K) cell volume reduction and (L) Hog1nuc responses over time. The lines represent means, and the shaded areas indicate standard deviations (std) from 2 to 3 biological replicates (BRs), each with approximately 100 single cells analyzed through time-lapse microscopy. Further details can be found in Figure S5.

pulsatile stress (Figures 2 and S1). We then implemented gradual cell stress stimulations and time-lapse microscopy to quantify cell volume change and Hog1 signaling activation dynamics in single cells over time. We found that cell volume reduction depends on the gradual dynamic of the stress (Figures 3 and S2). Interestingly, we uncovered that cell growth rate negatively correlates with cell volume reduction for different gradual stress conditions (Figures 4, S3, and S4), even when compared to the same total stress exposure (Figure S6). Our results revealed that cells grow optimally upon stress conditions that cause minimal cell volume reduction. Through implementing quantitative models of three different signaling mechanisms, we predicted the signatures of signaling activation dynamics under five distinct stress paradigms, namely linear, exponential, polynomials, pulsatile, and staircase stress (Figure 5). We subsequently compared these model predictions to our experimental measurements, confirming logarithmic signaling contributing to the Hog1 pathway response to sense the relative change in gradual stress over the background concentration over time (Figures 6 and S5).

We find that cell volume reduction in a stress dynamic-dependent manner impedes cell growth independent of the rising part of the Hog1 signaling activation, while prolonged signaling under gradual stress may help cells improve growth. This physiological signaling mechanism is significant because it induces persistent Hog1 activation upon gradual stimulations that maximizes cell survival in severe stress conditions and links cell morphology changes to growth phenotype. These results show that gradual dynamics of extracellular environments impact cell growth and cell volume and our study provides a quantitative framework to investigate what signaling pathways may be involved in these processes.

Our data establishes logarithmic signaling (Figure 7), a signal transduction mechanism of perceiving relative changes of extracellular stress, with a phenotypic consequence in yeast cells. Such signaling mechanism may be prevalent in pathways such as ERK, Wnt, NF-κB, Tgf-β, PI3K-Akt and may play important roles to regulate distinct cellular responses and functions during important biological processes relevant to human health and disease.[54–58]

Limitations of the study

This study revealed logarithmic signaling in the Hog1 pathway using time-lapse microscopy and observed a viability phenotype under high osmotic stress with varying dynamics. However, the molecular mechanism underlying logarithmic sensing remains unidentified and requires further investigation. Additionally, future experiments should distinguish between cell death and growth arrest to clarify their respective contributions to the observed viability phenotype.

RESOURCE AVAILABILITY

Lead contact

Further information and requests for resources should be directed to and will be fulfilled by the lead contact, Gregor Neuert (gregor.neuert@vanderbilt.edu).

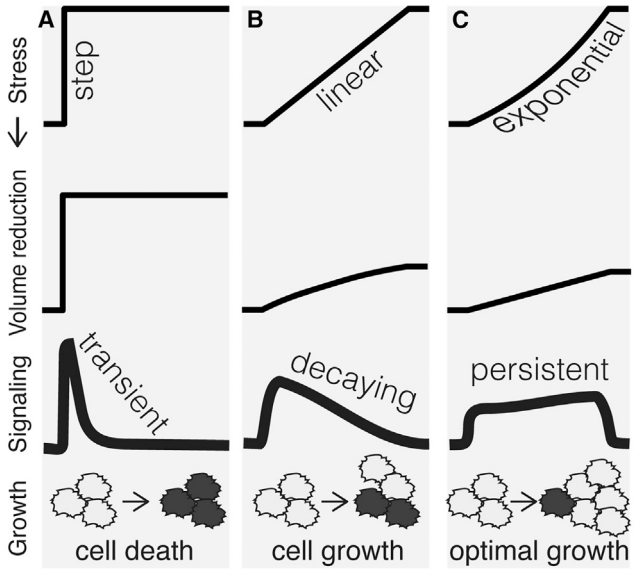

Figure 7. Gradual stress identified logarithmic signaling as a mechanism contributing to optimal cell growth

(A) Application of different cell stress profiles over time, in the form of (A) an acute step change, (B) a linear, and (C) an exponential stress, yield distinctive dynamics in signaling activation dynamics and phenotypes. Notably, (A) rapid step stress induces substantial cell volume reduction compared to the (B–C) gradual stress, while signaling persists longer with gradual stress compared to step stress. Compared to the standard paradigm in which the concentration of osmotic stress dictates cell growth, in this study we discovered that gradual stress, in a dynamic-dependent manner, influences cell volume reduction and signaling activation, which in turn dictates the cell growth phenotype.

Materials availability

This study did not generate new unique reagents.

Data and code availability

- The structured datasets generated during this study are available on Zenodo at https://doi.org/10.5281/zenodo.13883051.
- The custom codes generated during this study are available on Zenodo at https://doi.org/10.5281/zenodo.13883051.
- Any additional information required to reanalyze the data reported in this work paper is available from the lead contact upon request.

ACKNOWLEDGMENTS

GN is supported by NIH R01GM140240, and Vanderbilt Basic Science Dean's Faculty Fellow Endowed Chair. The authors thank Drs. Brian Munsky and Zachary Fox for their valuable discussions on the manuscript and Dr. Zachary Fox for his comments on the manuscript. This study used resources at the Advanced Computing Center for Research and Education (ACCRE) at Vanderbilt University, Nashville, TN (NIH S10 Shared Instrumentation Grant 1S10OD023680-01 (Meiler).

AUTHOR CONTRIBUTIONS

Conceptualization, H.J. and G.N; Methodology, H.J.; Software, H.J. and G.N.; Validation, H.J.; Formal Analysis, H.J.; Investigation, H.J.; Data curation, H.J.; Writing – original draft, H.J.; Writing – review and editing, H.J. and G.N.; Visualization, H.J.; Supervision, G.N., Project administration, H.J. and G.N.; Funding acquisition, G.N.

DECLARATION OF INTERESTS

Technology to generate gradual environmental changes is disclosed in a provisional patent application #VU22141PCT1.

STAR★METHODS

Detailed methods are provided in the online version of this paper and include the following:

- KEY RESOURCES TABLE
- METHOD DETAILS
  - Gradual cell stimulations paradigms
  - Concentrated stress, 5M NaCl in CSM
  - Yeast strain and cell culture
  - Cell growth measurements
  - Time-lapse microscopy
  - Image acquisition
  - Image segmentation
  - Quantification of cell growth rates
  - Quantification of cell volume change
  - Quantification of Hog1 nuclear localization
  - Quantitative modeling of different signaling mechanisms
- QUANTIFICATION AND STATISTICAL ANALYSIS
- ADDITIONAL RESOURCES

SUPPLEMENTAL INFORMATION

Supplemental information can be found online at https://doi.org/10.1016/j.isci.2024.111625.

Received: December 15, 2023
Revised: October 4, 2024
Accepted: December 16, 2024
Published: December 19, 2024

REFERENCES

1. Lim, W., Mayer, B., and Pawson, T. (2014). Cell Signaling: Principles and Mechanisms, 1 Edition (Taylor and Francis Group, LLC). Garland Science.
2. Neben, C.L., Lo, M., Jura, N., and Klein, O.D. (2019). Feedback regulation of RTK signaling in development. Dev. Biol. *447*, 71–89. https://doi.org/10.1016/j.ydbio.2017.10.017.
3. Nikolaev, S.I., Vetiska, S., Bonilla, X., Boudreau, E., Jauhiainen, S., Rezai Jahromi, B., Khyzha, N., DiStefano, P.V., Suutarinen, S., Kiehl, T.R., et al. (2018). Somatic Activating KRAS Mutations in Arteriovenous Malformations of the Brain. N. Engl. J. Med. *378*, 250–261. https://doi.org/10.1056/NEJMoa1709449.
4. Hata, A., and Chen, Y.G. (2016). TGF-β signaling from receptors to smads. Cold Spring Harbor Perspect. Biol. *8*, a022061. https://doi.org/10.1101/cshperspect.a022061.
5. Harvey, S.A., and Smith, J.C. (2009). Visualisation and Quantification of Morphogen Gradient Formation in the Zebrafish. PLoS Biol. *7*, e1000101. https://doi.org/10.1371/journal.pbio.1000101.
6. Hanahan, D. (2022). Hallmarks of Cancer: New Dimensions. Cancer Discov. *12*, 31–46. https://doi.org/10.1158/2159-8290.CD-21-1059.
7. Groß, A., Kracher, B., Kraus, J.M., Kühlwein, S.D., Pfister, A.S., Wiese, S., Luckert, K., Pötz, O., Joos, T., Van Daele, D., et al. (2019). Representing dynamic biological networks with multi-scale probabilistic models. Commun. Biol. *2*, 1–12. https://doi.org/10.1038/s42003-018-0268-3.
8. Romers, J., Thieme, S., Münzner, U., and Krantz, M. (2020). A scalable method for parameter-free simulation and validation of mechanistic cellular signal transduction network models. npj Systems Biology and Applications *6*, 1–13. https://doi.org/10.1038/s41540-019-0120-5.

9. Janes, K.A., and Lauffenburger, D.A. (2013). Models of signalling networks-what cell biologists can gain from them and give to them. J. Cell Sci. *126*, 1913–1921. https://doi.org/10.1242/jcs.112045.

10. Murugan, A., Husain, K., Rust, M.J., Hepler, C., Bass, J., Pietsch, J.M.J., Swain, P.S., Jena, S.G., Toettcher, J.E., Chakraborty, A.K., et al. (2021). Roadmap on biology in time varying environments. Phys. Biol. *18*, 041502. https://doi.org/10.1088/1478-3975/ABDE8D.

11. Zhang, J., Tian, X.-j., and Xing, J. (2016). Signal Transduction Pathways of EMT Induced by TGF-β, SHH, and WNT and Their Crosstalks. J. Clin. Med. *5*, 41. https://doi.org/10.3390/jcm5040041.

12. Handly, L.N., Yao, J., and Wollman, R. (2016). Signal transduction at the single-cell level: approaches to study the dynamic nature of signaling networks. J. Mol. Biol. *428*, 3669–3682.

13. Jashnsaz, H., Fox, Z.R., Hughes, J.J., Li, G., Munsky, B., and Neuert, G. (2020). Diverse cell stimulation kinetics identify predictive signal transduction models. iScience *23*, 101565. https://doi.org/10.1101/2020.01.28.923755.

14. Jashnsaz, H., Fox, Z.R., Munsky, B., Neuert, G., and Fox, R.,Z. (2021). Building predictive signaling models by perturbing yeast cells with time-varying stimulations resulting in distinct signaling responses. STAR Protoc. *2*, 100660. https://doi.org/10.1016/J.XPRO.2021.100660.

15. Thiemicke, A., and Neuert, G. (2023). Rate thresholds in cell signaling have functional and phenotypic consequences in non-linear time-dependent environments. Front. Cell Dev. Biol. *11*, 1124874. https://doi.org/10.3389/FCELL.2023.1124874.

16. Kubota, H., Noguchi, R., Toyoshima, Y., Ozaki, Y.-i., Uda, S., Watanabe, K., Ogawa, W., and Kuroda, S. (2012). Temporal Coding of Insulin Action through Multiplexing of the AKT Pathway. Mol. Cell *46*, 820–832. https://doi.org/10.1016/j.molcel.2012.04.018.

17. Madsen, R.R., and Vanhaesebroeck, B. (2020). Cracking the context-specific PI3K signaling code. Sci. Signal. *13*, eaay2940.

18. Mettetal, J.T., Muzzey, D., Gómez-Uribe, C., van Oudenaarden, A., and Gomez-Uribe, C. (2008). The Frequency Dependence of Osmo-Adaptation in Saccharomyces cerevisiae. Science *319*, 482–484. https://doi.org/10.1126/science.1151582.

19. Mitchell, A., Wei, P., and Lim, W.A. (2015). Oscillatory stress stimulation uncovers an Achilles heel of the yeast MAPK signaling network. Science *350*, 1379–1383. https://doi.org/10.1126/science.aab0892.

20. Muzzey, D., Gómez-Uribe, C.A., Mettetal, J.T., and van Oudenaarden, A. (2009). A Systems-Level Analysis of Perfect Adaptation in Yeast Osmoregulation. Cell *138*, 160–171. https://doi.org/10.1016/j.cell.2009.04.047.

21. Rahi, S.J., Larsch, J., Pecani, K., Katsov, A.Y., Mansouri, N., Tsaneva-Atanasova, K., Sontag, E.D., and Cross, F.R. (2017). Oscillatory stimuli differentiate adapting circuit topologies. Nat. Methods *14*, 1010–1016. https://doi.org/10.1038/nmeth.4408.

22. Shimizu, T.S., Tu, Y., and Berg, H.C. (2010). A modular gradient-sensing network for chemotaxis in Escherichia coli revealed by responses to time-varying stimuli. Mol. Syst. Biol. *6*, 382. https://doi.org/10.1038/msb.2010.37.

23. Sorre, B., Warmflash, A., Brivanlou, A.H., and Siggia, E.D. (2014). Encoding of temporal signals by the TGF-β Pathway and implications for embryonic patterning. Dev. Cell *30*, 334–342. https://doi.org/10.1016/j.devcel.2014.05.022.

24. Thiemicke, A., Jashnsaz, H., Li, G., and Neuert, G. (2019). Generating kinetic environments to study dynamic cellular processes in single cells. Sci. Rep. *9*, 10129.

25. Thiemicke, A., and Neuert, G. (2021). Kinetics of osmotic stress regulate a cell fate switch of cell survival. Sci. Adv. *7*, eabe1122.

26. Johnson, A.N., Li, G., Jashnsaz, H., Thiemicke, A., Kesler, B.K., Rogers, D.C., and Neuert, G. (2021). A rate threshold mechanism regulates MAPK stress signaling and survival. Proc. Natl. Acad. Sci. USA *118*, e2004998118. https://doi.org/10.1073/pnas.2004998118.

27. Zhang, C., Tu, H.-L., Jia, G., Mukhtar, T., Taylor, V., Rzhetsky, A., and Tay, S. (2019). Ultra-multiplexed analysis of single-cell dynamics reveals logic rules in differentiation. Sci. Adv. *5*, eaav7959. https://doi.org/10.1126/sciadv.aav7959.

28. Cai, Q., Ferraris, J.D., and Burg, M.B. (2004). Greater tolerance of renal medullary cells for a slow increase in osmolality is associated with enhanced expression of HSP70 and other osmoprotective genes. Am. J. Physiol. Ren. Physiol. *286*, F58–F67. https://doi.org/10.1152/ajprenal.00037.2003.

29. Heltberg, M.L., Krishna, S., and Jensen, M.H. (2019). On chaotic dynamics in transcription factors and the associated effects in differential gene regulation. Nat. Commun. *10*, 71. https://doi.org/10.1038/s41467-018-07932-1.

30. Fujita, K.A., Toyoshima, Y., Uda, S., Ozaki, Y.-I., Kubota, H., and Kuroda, S. (2010). Decoupling of Receptor and Downstream Signals in the Akt Pathway by Its Low-Pass Filter Characteristics. Sci. Signal. *3*, ra56. https://doi.org/10.1126/scisignal.2000810.

31. Goulev, Y., Morlot, S., Matifas, A., Huang, B., Molin, M., Toledano, M.B., and Charvin, G. (2017). Nonlinear feedback drives homeostatic plasticity in H2O2 stress response. Elife *6*, e23971. https://doi.org/10.7554/eLife.23971.

32. Granados, A.A., Crane, M.M., Montano-Gutierrez, L.F., Tanaka, R.J., Voliotis, M., and Swain, P.S. (2017). Distributing tasks via multiple input pathways increases cellular survival in stress. Elife *6*, e21415. https://doi.org/10.7488/DS/2043.

33. Briscoe, J., and Small, S. (2015). Morphogen rules: design principles of gradient-mediated embryo patterning. Development *142*, 3996–4009. https://doi.org/10.1242/DEV.129452.

34. Ashall, L., Horton, C.A., Nelson, D.E., Paszek, P., Harper, C.V., Sillitoe, K., Ryan, S., Spiller, D.G., Unitt, J.F., Broomhead, D.S., et al. (2009). Pulsatile Stimulation Determines Timing and Specificity of NF-κB-Dependent Transcription. Science *324*, 242–246.

35. Liu, T., Zhang, L., Joo, D., and Sun, S.-C. (2017). NF-κB signaling in inflammation. Signal Transduct. Targeted Ther. *2*, 17023–17029. https://doi.org/10.1038/sigtrans.2017.23.

36. Mokashi, C.S., Schipper, D.L., Qasaimeh, M.A., and Lee, R.E.C. (2019). A System for analog control of cell culture dynamics to reveal capabilities of signaling networks. iScience *19*, 586–596. https://doi.org/10.1016/j.isci.2019.08.010.

37. Oyler-Yaniv, A., Oyler-Yaniv, J., Whitlock, B.M., Liu, Z., Germain, R.N., Huse, M., Altan-Bonnet, G., and Krichevsky, O. (2017). A tunable diffusion-consumption mechanism of cytokine propagation enables plasticity in cell-to-cell communication in the immune system. Immunity *46*, 609–620. https://doi.org/10.1016/j.immuni.2017.03.011.

38. Twohig, J.P., Cardus Figueras, A., Andrews, R., Wiede, F., Cossins, B.C., Derrac Soria, A., Lewis, M.J., Townsend, M.J., Millrine, D., Li, J., et al. (2019). Activation of naïve CD4+ T cells re-tunes STAT1 signaling to deliver unique cytokine responses in memory CD4+ T cells. Nat. Immunol. *20*, 458–470. https://doi.org/10.1038/s41590-019-0350-0.

39. Chanaday, N.L., and Kavalali, E.T. (2018). Optical detection of three modes of endocytosis at hippocampal synapses. Elife *7*, e36097. https://doi.org/10.7554/eLife.36097.

40. Purvis, J.E., Karhohs, K.W., Mock, C., Batchelor, E., Loewer, A., and Lahav, G. (2012). p53 Dynamics Control Cell Fate. Science *336*, 1440–1444. https://doi.org/10.1126/science.1218351.

41. Adler, M., and Alon, U. (2018). Fold-change detection in biological systems. Curr. Opin. Struct. Biol. *8*, 81–89. https://doi.org/10.1016/J.COISB.2017.12.005.

42. Tendler, A., Wolf, B.C., Tiwari, V., Alon, U., and Danon, A. (2018). Fold-change Response of Photosynthesis to Step Increases of Light Level. iScience *8*, 126–137. https://doi.org/10.1016/j.isci.2018.09.019.

43. Young, J.W., Locke, J.C.W., and Elowitz, M.B. (2013). Rate of environmental change determines stress response specificity. Proc. Natl. Acad. Sci. USA *110*, 4140–4145. https://doi.org/10.1073/pnas.1213060110.

44. Brewster, J.L., and Gustin, M.C. (2014). Hog1: 20 years of discovery and impact. Sci. Signal. *7*, re7. https://doi.org/10.1126/scisignal.2005458.

45. Tatebayashi, K., Yamamoto, K., Tomida, T., Nishimura, A., Takayama, T., Oyama, M., Kozuka-Hata, H., Adachi-Akahane, S., Tokunaga, Y., and Saito, H. (2020). Osmostress enhances activating phosphorylation of Hog1 MAP kinase by mono-phosphorylated Pbs2 MAP2K. EMBO J. *39*, e103444. https://doi.org/10.15252/embj.2019103444.

46. Tanaka, K., Tatebayashi, K., Nishimura, A., Yamamoto, K., Yang, H.Y., and Saito, H. (2014). Yeast Osmosensors Hkr1 and Msb2 Activate the Hog1 MAPK Cascade by Different Mechanisms. Sci. Signal. *7*, ra21. https://doi.org/10.1126/scisignal.2004780.

47. Macia, J., Regot, S., Peeters, T., Conde, N., Solé, R., Posas, F., and Sole, R. (2009). Dynamic Signaling in the Hog1 MAPK Pathway Relies on High Basal Signal Transduction. Sci. Signal. *2*, ra13. https://doi.org/10.1126/scisignal.2000056.

48. Lee, J., Reiter, W., Dohnal, I., Gregori, C., Beese-Sims, S., Kuchler, K., Ammerer, G., and Levin, D.E. (2013). MAPK Hog1 closes the S. cerevisiae glycerol channel Fps1 by phosphorylating and displacing its positive regulators. Genes Dev. *27*, 2590–2601. https://doi.org/10.1101/gad.229310.113.

49. Mattison, C.P., and Ota, I.M. (2000). Two protein tyrosine phosphatases, Ptp2 and Ptp3, modulate the subcellular localization of the Hog1 MAP kinase in yeast. Genes Dev. *14*, 1229–1235. https://doi.org/10.1101/gad.14.10.1229.

50. Miermont, A., Waharte, F., Hu, S., McClean, M.N., Bottani, S., Léon, S., and Hersen, P. (2013). Severe osmotic compression triggers a slowdown of intracellular signaling, which can be explained by molecular crowding. Proc. Natl. Acad. Sci. USA *110*, 5725–5730. https://doi.org/10.1073/pnas.1215367110.

51. Babazadeh, R., Adiels, C.B., Smedh, M., Petelenz-Kurdziel, E., Goksör, M., Hohmann, S., Wood, J.M., Chen, R.E., Thorner, J., Saito, H., et al. (2013). Osmostress-Induced Cell Volume Loss Delays Yeast Hog1 Signaling by Limiting Diffusion Processes and by Hog1-Specific Effects. PLoS One *8*, e80901. https://doi.org/10.1371/journal.pone.0080901.

52. Altenburg, T., Goldenbogen, B., Uhlendorf, J., and Klipp, E. (2019). Osmolyte homeostasis controls single-cell growth rate and maximum cell size of Saccharomyces cerevisiae. NPJ Syst. Biol. Appl. *5*, 34. https://doi.org/10.1038/s41540-019-0111-6.

53. Talemi, S.R., Tiger, C.F., Andersson, M., Babazadeh, R., Welkenhuysen, N., Klipp, E., Hohmann, S., Schaber, J., Nordlander, B., Kruger, R., et al. (2016). Systems Level Analysis of the Yeast Osmo-Stat. Sci. Rep. *6*, 30950. https://doi.org/10.1038/srep30950.

54. Cohen-Saidon, C., Cohen, A.A., Sigal, A., Liron, Y., and Alon, U. (2009). Dynamics and variability of ERK2 response to EGF in individual living cells. Mol. Cell *36*, 885–893. https://doi.org/10.1016/j.molcel.2009.11.025.

55. Goentoro, L., and Kirschner, M.W. (2009). Evidence that fold-change, and not absolute level, of beta-catenin dictates Wnt signaling. Mol. Cell *36*, 872–884. https://doi.org/10.1016/j.molcel.2009.11.017.

56. Lee, R.E.C., Walker, S.R., Savery, K., Frank, D.A., and Gaudet, S. (2014). Fold Change of Nuclear NF-κB Determines TNF-Induced Transcription in Single Cells. Mol. Cell *53*, 867–879. https://doi.org/10.1016/J.MOLCEL.2014.01.026.

57. Frick, C.L., Yarka, C., Nunns, H., and Goentoro, L. (2017). Sensing relative signal in the Tgf-β/Smad pathway. Proc. Natl. Acad. Sci. USA *114*, E2975–E2982. https://doi.org/10.1073/pnas.1611428114.

58. Lyashenko, E., Niepel, M., Dixit, P.D., Lim, S.K., Sorger, P.K., and Vitkup, D. (2020). Receptor-based mechanism of relative sensing and cell memory in mammalian signaling networks. Elife *9*, e50342. https://doi.org/10.7554/eLife.50342.

59. Neuert, G., Munsky, B., Tan, R.Z., Teytelman, L., Khammash, M., and van Oudenaarden, A. (2013). Systematic Identification of Signal-Activated Stochastic Gene Regulation. Science *339*, 584–587. https://doi.org/10.1126/science.1231456.

60. Kesler, B., Li, G., Thiemicke, A., Venkat, R., and Neuert, G. (2019). Automated cell boundary and 3D nuclear segmentation of cells in suspension. Sci. Rep. *9*, 10237. https://doi.org/10.1038/s41598-019-46689-5.

61. Munsky, B., Li, G., Fox, Z.R., Shepherd, D.P., and Neuert, G. (2018). Distribution shapes govern the discovery of predictive models for gene regulation. Proc. Natl. Acad. Sci. USA *115*, 7533–7538. https://doi.org/10.1073/pnas.1804060115.

STAR★METHODS

KEY RESOURCES TABLE

REAGENT or RESOURCE	SOURCE	IDENTIFIER
Critical commercial assays		
New Era Syringe Pumps	https://www.syringepump.com/index.php	New Era, NE-1200
Tubing	Scientific Commodities	Catalog#: BB31695-PE/4
Dispensing Needles	https://www.cmlsupply.com/dispensing-needle-20ga-1-0-tip-yellow/	CML Supply 20ga x 1.0″ Yellow Blunt Tip Dispensing Fill Needles (SKU:901-20-100, MPN:901-20-100)
Acrylic Side	Grace BIO-LABS	Custom 0.125 Clear Acrylic Side w/3-Ports (product code: RD440562)
T-shape Adhesive Spacer	Grace BIO-LABS	SecureSeal Adhesive Spacer, "T", 1L Adhesive, 44040 (product code: 440556)
Deposited data and codes		
Yeast cell growth data	This study	OD600 measurements
Cell volume and signaling data	This study	cell-volume-signaling-data
Data and codes for gradual stress profiles	This study	cell-stimulation-profiles
Analysis codes	This study	MATLAB codes
Experimental models: organisms/strains		
Saccharomyces cerevisiae (BY4741)	Thiemicke et al., 2019[24]	*MAT***a** *his3Δ1 leu2Δ0 met15Δ0 ura3Δ0*
Saccharomyces cerevisiae (Hog1-YFP)	Johnson et al., 2021[26]	*MAT***a** *his3Δ1 leu2Δ0 met15Δ0 ura3Δ0 HOG1- YFP::HIS3*
Software and algorithms		
Algorithms to set the pump profiles	Thiemicke et al.[24]	Algorithms to generate gradual cell stimulation profiles
Codes and data for pump profiles	This study	cell-stimulation-profiles
Codes to calculate the inoculation volumes for cell cultures	Jashnsaz et al.[14]	Jashnsaz_et_al_dir07_CellGrowth
Image processing codes	Neuert et al.[59] and Kesler et al.[60]	https://osf.io/kwbe6/
Cell growth, volume and signaling data analysis codes	This study	https://doi.org/10.5281/zenodo.13883051
MATLAB		programming and computing platform to analyze data, develop algorithms, and build models
Other		
Microscope	Nikon	Nikon Eclipse Ti
Perfect Focus System (PFS)	Nikon	TI-PFS-CON 596216
X-cite fluorescent light source	Excelitas	series 120 Q
Fluorescent filter for YFP	Semrock	YFP-2427B-NTE
100x VC DIC lens	Nikon	MRD01901
Orca Flash 4v2 CMOS camera	Hamamatsu	C11440-22CU
Automated XYZ high-resolution stage	ASI	ME-2000
Microscope cover glass	Fisherbrand	12-545-E 22x50-1

METHOD DETAILS

Gradual cell stimulations paradigms

To investigate dynamic responses and phenotypes in yeast cells under various gradual stress conditions, we meticulously designed and executed gradual stress profiles spanning a wide range of concentrations and rates. We employed sodium chloride (NaCl,

Sigma-Aldrich, S7653) concentration changes based on polynomial and exponential increases over time, ultimately reaching one of the final concentrations of 0.10M, 0.20M, 0.40M, 0.60M, or 0.80M over a 25-min period in independent experiments (Figures 3C and S3A).[14,24,26]

In our experimental setup, we employed programmable syringe pumps (New Era Pump Systems, NE-1200) capable of operating in 251 phases, enabling the creation of profiles comprising 250 linear concentration intervals, each lasting 6 s. This design ensured a continuous, monotonically increasing concentration profiles for all conditions in this study. By progressively increasing the rate between intervals, we achieved the desired rising concentration profiles throughout the entire treatment duration. During each 6-s interval, the pump consistently delivered the stress by introducing the appropriate volume of concentrated stress solution, while correcting for both the added and removed volumes. The former step delivered the concentrated stress to a mixing flask, while the latter delivered the changing concentration to the cells over time.

These gradual NaCl concentrations were then applied to yeast cells in real time to evaluate their impact on cell growth, cell volume change, and Hog1 kinase nuclear localization ($Hog1^{nuc}$) phenotypes. Additionally, our experimental setup allowed us to implement step-like profiles and pulsatile and staircase stresses by switching the extracellular medium between different fixed final concentrations of NaCl.[14,24,26]

Concentrated stress, 5M NaCl in CSM

We prepared a concentrated stress of 5M NaCl in 1X CSM (yeast growth media) for use in all experiments in this study. To create this solution, we dissolved 292.2 g of sodium chloride (NaCl) in 850 mL of CSM 1X, followed by autoclaving. We then adjusted the final volume to 1,000 mL using 50 mL pipettes and additional CSM. CSM 1X was prepared using 75mL CSM 10X (5.925 g CSM, Formedium DCS0019, in 750 mL ddH2O), 75mL YNB 10X (51.75 g Yeast Nitrogen Base w/o Amino Acids, YNB, Formedium, CYN0410 in 750 mL ddH2O), 75 mL Glucose 20% (150 g Glucose, Fisher, Dextrose Anhydrous 147, M-15722 in 750 mL ddH2O), and 525mL ddH2O.[14]

Yeast strain and cell culture

We employed *Saccharomyces cerevisiae* BY4741 (MATa; his3Δ1; leu2Δ0; met15Δ0; ura3Δ0) for our experiments. To assess the nuclear enrichment of Hog1 in response to osmotic stress at the single-cell level, we utilized a yellow-fluorescent protein (YFP) tag, which we introduced to the C-terminus of the endogenous Hog1 protein in BY4741 cells via homologous DNA recombination.[26]

In preparation for our experiments, yeast cells from a stock stored at −80°C were streaked onto a complete synthetic media plate three days prior to the study. The day before the experiment, a single colony from the CSM plate was selected and used to inoculate 5 mL of CSM medium to establish a pre-culture. After 6–12 h, we measured the optical density (OD) of the pre-culture and diluted it into fresh CSM medium to achieve an OD of 0.5 the following morning.

Cell growth measurements

In this study, we exposed yeast cells to various gradual osmotic stress conditions to investigate their effects on cell growth phenotypes. Yeast cell cultures were grown until they reached the exponential growth phase (OD600 = 0.5) before subjecting them to different stress conditions. We monitored cell growth by measuring optical density of cell culture at 600 nm (OD600) over time, both before and after each stress treatment. Based on these measurements, the growth phenotype in our study reflects an average of cells with normal growth, abnormal growth, and dead cells. Our experiments involved repetitive NaCl stress treatments, including long pulses, short pulses, linear increases, and exponential increases along proper controls to account for stress duration, integrated stress exposure, and cell density, with each reaching a final concentration of 3M NaCl. Detailed profiles for each condition can be found in Figures 2 and S1. To implement these conditions, we added a total of 21.75 mL of concentrated stress (5M NaCl in CSM) to 14.5 mL of cells in CSM.

For pulsatile stress treatments, the entire 21.75 mL of 5M NaCl was introduced to the cells in a mixing flask at once. In the case of linear and exponential stress treatments, the 21.75 mL of 5M NaCl was gradually delivered to the cells over time using a 20 mL BD syringe (BD, 309628) mounted on a syringe pump. Introducing 21.75 mL of 5M NaCl either in a single acute stress event (pulsatile stress) or gradually over 120 min (linear and exponential stress) leads to distinct cell dilution profiles thus distinct cell density changes throughout the 2-h treatment duration (Figure 2A). These variations may have implications for post-stress cell growth. The experiment presented in Figure 2D serves as a control to account for this potential effect. During the gradual stress applications, the syringe pump functioned according to the calculated linear or exponential profile for the delivery of each over the 90-min treatment period. The dispensed volume selections were determined by the capacity of the 20 mL BD syringes, which allowed for a 21.75 mL fill volume for each experiment without the need for refilling during the treatment.

After each stress treatment, we removed the NaCl by filtering the cells using 0.45 μm filters (Filter Membranes, Millipore, HAWP09000) and a glass vacuum system, and then resuspended them in 40 mL of fresh CSM. We incubated the cells and measured OD600 during the next 5 h at various time points: 15 min, 1 h, 1 h and 45 min, 2 h and 30 min, 3 h and 15 min, 4 h, and 4 h and 45 min post-incubation. Throughout the experiments, we ensured homogeneous mixing by constantly shaking the cells at 200 rpm in a 30°C incubator, and we maintained the growth media and concentrated stress within the same 30°C incubator for temperature control.

Time-lapse microscopy

A volume of 1.5 mL of yeast cells at OD600 = 0.5 were centrifuged, the supernatant was removed, and the remaining cell pellets (approximately 40 μL) from three centrifugation tubes were combined into one, and loaded into the flow chamber. After loading the cells into the flow chamber, the chamber was attached to the microscope, and a 5-min incubation period allowed the cells to adhere to the Concanavalin (Sigma, L7647) coverslip. The flow chamber configuration comprised an 1/8″ Clear Acrylic Slide with three holes (Grace Bio-labs, 44562), a 0.17 μm thick T-shape SecureSeal Adhesive spacer (Grace Bio-labs, 44560, 1 L 44040, R&D), a Microscope Cover Glass (Fisher Scientific, 12545E, No 1 22 × 50 mm), and Micro medical tubing (Scientific Commodities Inc., BB31695-PE/4, 100 feet, 0.72 mm ID × 1.22 mm OD). The cover glass had been coated with a solution of 0.1 mg/mL ConA in H2O.

NaCl stress profiles were established using Syringe Pumps, consistent with the procedures described in previous sections. To facilitate acute stress, flask 1 contained CSM medium with a predetermined NaCl concentration. For gradual stimulations, the mixing flask initially held media without NaCl at time zero, and we generated concentration profiles by pumping 5M NaCl CSM media into the mixing flask using a syringe pump. These media changes were continuously mixed on a magnetic stir plate to achieve the desired profiles to stress the yeast cells.

Image acquisition

For the quantification of nuclear enrichment of Hog1 terminal kinase in individual yeast cells as an indicator of pathway activation, we employed a strain in which a yellow-fluorescent protein (YFP) was integrated at the C-terminus of the endogenous Hog1 protein in *Saccharomyces cerevisiae* BY4741 yeast, using homologous DNA recombination.

Our imaging setup consisted of an inverted microscope, specifically the Nikon Eclipse Ti, which was equipped with several components, including perfect focus (Nikon), a 100× VC DIC lens (Nikon), a YFP fluorescent filter from Semrock, an X-cite fluorescent light source (Excelitas), and an Orca Flash 4v2 CMOS camera from Hamamatsu. The entire system was controlled via the Micro-Manager program.

To capture images, we conducted the following steps:

Utilizing the microscope's xy-plane movement, we selected a field of view that exhibited an optimal density of yeast cells within a single z-plane. The z-focus was carefully adjusted to visualize the boundary of most cells, appearing as a white ring. Time-lapse images were recorded, encompassing both bright-field images, taken at intervals of every 10 s, and fluorescent channel images, acquired at intervals of every minute.

Image segmentation

The published articles[24,26,59–61] include the image processing codes for cell segmentation and quantification that are used to analyze the cell volume change and Hog1 nuclear localization data during this study. Cell segmentation was performed in 2D, and the cell area was then converted into volume. The change in cell volume is calculated as the ratio of the volume at a given time to the volume before osmotic stress. To account for normalized volume changes, the area change is converted into volume change using the formula $(V(t)/V(t=0))=(A(t)/A(t=0))^{1.5}$ (23). The codes for cell segmentation are available at https://osf.io/kwbe6/.

Quantification of cell growth rates

To determine cell growth rates, we employed a fitting procedure to the OD600 measurements, from which we calculated the doubling times and growth rates. This involved fitting the OD600 data to doubling functions, calculating doubling times and growth rates, and normalizing these values with respect to the control condition to analyze the impact of various stress conditions on cell growth.

The cell growth data were fitted using the following mathematical function:

$$y(t) = y0 * 2^{\frac{t}{T}} \quad \text{(Equation 1)}$$

Where:

(1) $y(t)$ represents the OD600 measurements at time t.
(2) $y0$ is the initial OD600 value for each condition.
(3) T represents the doubling time, which is the time it takes for the OD600 to double.
(4) The reciprocal of T represents the cell growth rate.

We independently fitted data from each section for each biological replicate (Figures 2 and S1). For each condition, we performed 30 different fits. The resulting doubling times and growth rate values are obtained as averages of the fit values from these 30 independent fits.

To facilitate comparison, we normalized the growth rate values with respect to the mean growth rate observed under control conditions, which involved no NaCl. This normalization allows us to assess the relative changes in growth rates induced by the different stress conditions.

Quantification of cell volume change

In this study, the assessment of cell volume changes involved two main quantities.

(1) *Relative Cell Volume Changes Over Time:* We quantified the dynamics of cell volume change over time, normalized to the initial timepoints just before the application of each stress condition. This measure allowed us to track how cell volume evolved under different gradual stress.
(2) *Relative Cell Volume Reduction Over Time:* This specific metric was introduced to quantify cell volume change under each stress condition compared to that observed under a no-salt control condition. It was defined as the difference between cell volume changes under a given condition and the baseline cell volume expansion that occurs in standard growth media over time.

To obtain the relative cell volume reduction data, we subtracted the cell volume change under each stress condition from that under the no-salt control condition.

For the cell volume reduction data, we applied polynomial functions to describe the dynamics and compare cell volume reduction to cell stress dynamics. The fitting function took the following form:

$$y(t) = \begin{cases} 0, for \quad t<0 \\ y_{max} * \left(\frac{t}{T}\right)^k, for\ 0 \le t \le T \\ y_{max}, for \quad T<t \end{cases} \quad \text{(Equation 2)}$$

Where:

(1) $y(t)$ represents the cell volume reduction over time t.
(2) T is a fixed value of 25 min, as it was the duration of the stress period.
(3) y_{max} stands for the maximum volume reduction achieved for each specific condition.
(4) k corresponds to the polynomial order.

We independently fitted the data for each condition between time points 0 and 25 min. For each condition, we conducted 30 different fits, and the values of k and y_{max} were determined as averages based on the outcomes of these 30 independent fits. For the results presented in Figures 4C–4G and S3D, we used the following fitting function for the polynomial part:

$$y(t) = y_{max} * \left(\frac{t}{25+\tau}\right)^k \quad \text{(Equation 3)}$$

Where, τ is a free parameter that is introduced with its value constrained to the range [−2, 2] in units of minutes, to account for the small delay or expansion that was observed in the measured cell volume data. For example, $\tau = 0$ corresponds to the scenario where $y(t)$ reaches its maximum value of y_{max} at $t = 25$ minutes.

We examined two key aspects of cell volume change: the maximum cell volume reduction and the total cell volume reduction, both assessed over the 25-min stress period. This analysis allowed us to quantitatively capture the overall trends in cell volume dynamics under the various stress conditions.

Quantification of Hog1 nuclear localization

In our study, quantification of Hog1 nuclear localization is a crucial aspect of understanding the signaling dynamics within yeast cells subjected to various gradual stress. This quantification involves the calculation of the ratio of Hog1 signal derived from pixels representing the nucleus of individual cells to the total signal from the entire cell, with corrections made for the image background and photobleaching of the fluorescent signals over time. At the single-cell level and over time, we employ the following formula to quantify Hog1 nuclear localization using the nuclear, total cell, and image background signals over time:

$$H(t) = \frac{Signal_{Nuclear} - Signal_{ImageBackground}}{Signal_{TotalCell} - Signal_{ImageBackground}} = \frac{\frac{I_n(0)}{I_n(t)} * I_N(t) - \frac{I_b(0)}{I_b(t)} * I_B(t)}{\frac{I_t(0)}{I_t(t)} * I_T(t) - \frac{I_b(0)}{I_b(t)} * I_B(t)} \quad \text{(Equation 4)}$$

Here, the subscripts (N/n, T/t, B/b) correspond to (nuclear, total cell, image background) regions for a given single cell. We use capital letters (I_N, I_T, I_B) to denote the raw fluorescent signals from these regions. Meanwhile, lowercase letters ($I_n(t), I_t(t), I_b(t)$) represent the double-exponential decaying function fits for these signals obtained from pre-stress and the end of trajectories, modeling the photobleaching decay, while ($I_n(0), I_t(0), I_b(0)$) are the values at the first timepoint. It's important to note that in all conditions we maintain stress at fixed final concentrations for at least 25 min allowing Hog1 activities to adapt to pre-stress levels during these fits, allowing for accurate quantification of nuclear localization over time. We quantified Hog1 nuclear localization as Hog1nuc (t) = H(t) – H(0), where H(0) is the value at pre-stress timepoint.

This analysis plays a crucial role in correcting for the decay in fluorescent signal attributable to photobleaching, a phenomenon that can impact the accuracy of Hog1 nuclear localization measurements. For our control condition (CSM growth media with 0M NaCl), the method effectively achieves a constant Hog1nuc(t) value of 0 over time. However, the quantification of nuclear localization is influenced by the photobleaching events associated with the fluorescent protein used to label Hog1.

To address this issue and ensure accurate quantification, we conducted additional control experiments involving step-like stimulations applied to the cells at two distinct time points, namely t = 12 min and t = 20 min (Figures S2A–S2C). These experiments resulted in an additional 12 and 20 fluorescent images captured before the change in stress, compared to experiments in which we applied the step stress at t = 0. The Hog1nuc(t) values obtained from these experiments, using the aforementioned method, exhibited variations in signaling levels.

In response to these observed variations, we undertook supplementary experiments to empirically correct for the impact of photobleaching in Hog1nuc quantification. Specifically, we conducted nine experiments involving a step-like change of NaCl concentration to 0.6M at t = 0, each with an increasing number of pre-stress photobleaching snapshots taken (Figures S2D–S2G). This resulted in varying levels of Hog1nuc, depending on the number of pre-stress photobleaching snapshots.

To quantify these outcomes, we employed a fitting procedure to establish a relationship between the Hog1nuc values and the number of pre-stress photobleaching snapshots. Importantly, all our experiments involved the acquisition of fluorescent signal data at 1-min intervals, providing us with a quantitative factor to correct Hog1nuc signal over time (Figures S2H–S2J). This correction procedure ensures that the impact of photobleaching on Hog1 nuclear localization is appropriately accounted for in our analyses.

Similar to cell volume reduction data, we applied polynomial functions to describe the rising dynamics of $Hog1^{nuc}$ data over time and compare them to that of cell volume reduction and cell stimulations. The fitting function is given by Equation 2, where in these fits, we fix T to the value of time (in units of minutes) at which $Hog1^{nuc}$ reaches its maximum value. The results from these analyses are presented in Figures 4 and S4.

Quantitative modeling of different signaling mechanisms

To establish a relationship between time-dependent stress and the resulting signaling response dynamics, we developed a series of quantitative models to investigate various signaling mechanisms. Our goal was to predict the signaling response to different gradual stress accurately. To conduct a comprehensive analysis, we compared the behaviors of the following models.

(1) *Linear signaling:* This model is based on rate sensing, where the cellular response is directly proportional to the rate of change in the stress over time. In this model, we describe the signaling response as the first time-derivative of the stress profile.

$$R \propto \frac{d}{dt} s(t) \qquad \text{(Equation 5)}$$

(2) *Logarithmic signaling:* This model is based on relative rate sensing, in which the response is proportional to the relative change in stress concerning the background concentration over time. In this model, we describe the signaling response as the ratio of the first time-derivative of the stress divided by the stress concentration over time.

$$R \propto \frac{d}{dt} \log(s(t)) = \frac{ds(t)}{dt} \frac{1}{s(t)} \qquad \text{(Equation 6)}$$

We considered various gradual stress functions, as shown in Figure 5, and quantified the response from each model using each of the three approaches. Specifically, we numerically simulated concentration values at pre-specified timepoints and from those values we calculated the rate of change as difference in concentration values between adjacent timepoints. We used these values under gradual stress profiles to calculate responses for each model as described above. We then applied a 3-point moving average to smooth the responses.

QUANTIFICATION AND STATISTICAL ANALYSIS

Table 1 describes the biological replica and number of cells from all replica combined.

Figure 2 contains three biological replica for each experiment. The doubling times is the mean and std from fits to the grows curves of each replica experiment.

Figures 3E and 3F represent the mean and standard deviation (std) from 2 or 3 biological replicates, each consisting of approximately 100 single cells observed through live cell time-lapse microscopy.

In Figure 4, the x axis displays the mean and standard deviation (std) of volume reduction values (both maximum and total reductions) under control, step, linear, and exponential stress for five different final concentrations (C_{max} = 0.1M, 0.2M, 0.4M, 0.6M, and 0.8M), each normalized to the step condition with the greatest cell volume reduction (see Figure S3E). The y axis illustrates the mean

and std of cell growth rates under control, step, linear, and exponential stress conditions, normalized to the control condition with the highest cell growth rate values. Values from three biological replicates at post-1st-stress and post-2nd-stress are aggregated for this quantification (see Figures 2G–2I).

Figure 5, the lines represent means, and the shaded areas indicate standard deviations (std) from 2 to 3 biological replicates (BRs), each with approximately 100 single cells analyzed through time-lapse microscopy.

ADDITIONAL RESOURCES

For complete details on the protocol, please refer to https://star-protocols.cell.com/protocols/786.